Near-field optics and spectroscopy for molecular nano-imaging

SATOSHI KAWATA,[1,3] YASUSHI INOUYE[2,3] AND
TARO ICHIMURA[2]

Application of near-field optical microscopy with a sharp metallic probe to Raman spectroscopy brings microanalysis of materials to their nano-identification and imaging. The local plasmon polariton excitation on the probe tip results in the localization and amplification of the optical field at the vicinity of the tip. The tip-enhanced near-field Raman spectroscopy has analyzed DNA base molecules and single-walled carbon nanotubes (SWNTs) with the nanometric spatial resolution and sufficient sensitivity. Combined with tip pressurization and nonlinear effects, the tip-enhanced near-field Raman spectroscopy gives additional spectral information or improves the spatial resolution and sensitivity. This article introduces the recent progresses on the tip-enhanced near-field Raman spectroscopy and imaging.

Keywords: near-field optics, molecular nano-imaaging

1. Introduction

Photons could be converged in a finite volume through optical elements, such as an objective lens. The minimum size of the focused spot could be as small as half of the wavelength, due to the diffraction of the light wave (= diffraction limit). We can observe and analyze specimens with submicron resolution by optical microscopy in the visible region. It has been desired to realize optical microscopy with nanometric spatial resolution beyond the diffraction limit, so that various types of spectroscopic techniques, which give rich infor-mation of molecules and crystals, could be utilized. It would greatly contribute to the advances of nanosciences and nanotechnology. To

[1]Department of Applied Physics, Graduate School of Engineering, Osaka University, 2-1 Yamadaoka, Suita, Osaka 565-0871, Japan
[2]Graduate School of Frontier Biosciences, Osaka University, 1-3 Yamadaoka, Suita, Osaka 565-0871, Japan
[3]RIKEN, 2-1 Hirosawa, Wako, Saitama 351-0198, Japan

realize this attractive tool, we have to break through the diffraction limit. Near-field optical microscopy has been a promising tool to address this issue since the first experiment in 1984[1]. In the progress of the near-field microscopy[2,3], an apertureless metallic probe with a sharp apex has been proved to give the best spatial resolution among several types of probes[4]. The key role is played by the local enhancement of optical field in the nanometric vicinity of a light-irradiated metallic tip, through the excitation of local plasmon-polariton. The local field acts as a nanometric light-source for molecular imaging with a super resolution far beyond the diffraction limit. It is possible to utilize this nano light-source for many types of optical spectroscopy. In particular, Raman scattering spectroscopy assisted by the tip enhancement effect has proved to be a very powerful technique of molecular nano-analysis[5–10] (see Section 3). In addition to the Raman signal amplification, the tip chemically and mechanically affects the target molecules, resulting in the additional spectral changes[11] (See Section 4). Very recently, it has been verified that nonlinear Raman scattering combined with the near-field probe gives Raman images with a higher spatial resolution and detection sensitivity[12,13] (See Section 5).

2. Nano light source: Exceeding the diffraction limit

Fine structures with dimensions smaller than the wavelength of the illuminating light make evanescent photons localized in their proximity[14]. An evanescent photon possesses a wavenumber larger than that of propagating photons ($= 2 \pi/\lambda$) in one or two directions, and, therefore, possesses an imaginary wavenumber in the orthogonal direction. A photon with an imaginary wavenumber cannot propagate in that direction, and is localized near the fine structure. The increased wavenumber corresponds to a photon with a shorter wavelength. This shorter wavelength of the evanescent photons is comparable to the size of the structure, as well as the penetration length of the evanescent photons in the direction orthogonal to the structure. The evanescent photons are thus confined in the local space[15].

A near field probe with a nano-scaled structure locally generates and effectively confines evanescent photons near the tip. Several types of near-field probes, *e.g.* apertureless metallic probe, apertured probe, laser-trapped particle etc., play essentially the same roles in the near-filed microscopy. Recently, the apertureless metallic probe has been proved to be the most powerful for both spatial resolution and sensitivity. To understand the near field effect of the apertureless metallic probe, it is considered that a tip of probe with curvature much smaller than the wavelength of propagating light is close to a

dielectric substrate, and that the gap is irradiated with electromagnetic wave in the optical region. Since the dimension of the whole system consisting of the tip, the substrate and the gap is small compared to the wavelength, the phase retardation can be neglected. The electromagnetic wave can be considered to be spatially static, while it oscillates in time domain with exp($-i\omega t$). Under this so-called 'quasi-static' approximation, the external electric field applies an alternating voltage to the gap of the probe and the substrate. Equipotential planes lie on the surfaces of the probe and on the substrate. Many other equipotential planes exist between the probe and the substrate. These equipotential planes converge in the small gap just below the tip apex. Since the electric field is given by the spatial gradient of the electric potential, the electric field is locally strong in the gap. This effect, which is referred to as 'lightning rod effect', leads to confinement of the photons in the gap [16]. Semiconductive or dielectric tips also induce this effect.

The metallic tips contain conductive 'free electrons'. The electrons collectively oscillate at the surface of the metallic structures and resonantly couple to the external electric field. The quantum of the induced oscillation is called 'surface plasmon polariton'. The light propagating in space cannot excite the plasmon because of the wavenumber mismatch between the light and the plasmons, whereas nanoscaled structures including the nanometric tip can effectively induce the plasmon polaritons and confine the electric fields in the local vicinity. Figure 1(a) shows the local field distribution near a metallic probe tip calculated via the finite-difference time-domain (FDTD) method, which considers the phase retardation in the area
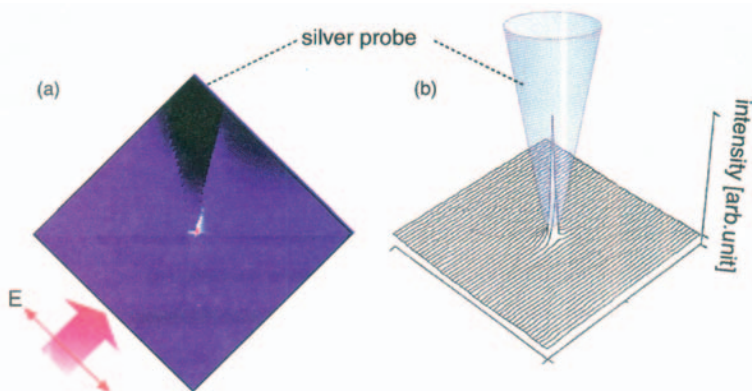

Fig. 1. Intensity distribution of enhanced electric field localized at a silver probe tip (a) in a plane containing the tip axis and (b) on a dielectric substrate, calculated with the FDTD method.

concerned[17]. It is seen that the optical field is highly confined into a tiny volume near the tip end. Besides the spatial confinement of the field, the optical field is strongly amplified by a factor of 50 at the maximum. This is attributed to the induced plasmons. Figure 1(b) shows a light intensity distribution on the dielectric substrate. Figure 1 shows the three-dimensional confinement of the optical field and an amplification of the light intensity in the confined spot. The size of the spot is comparable to that of the probe tip.

It has been shown that a metallic probe highly localizes and strongly amplifies optical field through the resonance effect of the nano-scaled structures and the plasmon polaritons. This concept has made it possible to optically observe the nanometric samples with a nanometric spatial resolution. Since our first proposal of this concept in 1994[4], many groups have applied it to spectroscopic measurement. There have been lots of studies aiming at optimization of the probe shape to improve both the localization and enhancement. Several reports suggested that a tip truncated to a finite size (< wavelength) gives a strong enhancement[18–20]. It is possible to fabricate a designed structure by using a focused ion beam (FIB).

3. Tip enhanced near field Raman spectroscopy

The metallic probe provides us a nano-scaled light source to realize optical spectroscopy with nanometric spatial resolution. Indeed, many scientists reported the local amplification of light emission due to quantum interaction such as fluorescence[21,22], two-photon-excited fluorescence[23], infrared absorption[24–26], and Raman scattering[5–10]. In particular, the tip enhancement of Raman scattering allows for nanoscale vibrational spectroscopy; hence, it is a promising tool that acquires chemical information on molecular species and its conformation, with nanometric spatial resolution. In the tip-enhanced near-field Raman spectroscopy, the tip enhancement is not only helpful for the spatial resolution but also indispensable to efficiently induce the Raman scattering process, where the scattering cross-section is extremely small ($\sim 10^{-30}$ cm^2) compared to those of fluorescence ($\sim 10^{-16}$ cm^2) and infrared absorption ($\sim 10^{-20}$ cm^2). It takes too much time to measure Raman scattering signals without the help of the plasmonic field-enhancement. This idea is actually analogous to the well-known surface enhanced Raman scattering (SERS), in which Raman scattering is amplified by a colloidal metallic nanoparticles or rough metal surfaces[27–29]. Therefore, the tip enhancement of Raman scattering can be regarded as a SERS effect with a single tip structure.

Figure 2 shows a schematic illustration of local enhancement of Raman scattering with a metallic probe. The incident field is strongly amplified by the metallic tip in the focused spot, and induces Raman scattering in the molecules located near the tip. As the *z*-polarized component of the electric field along the tip axis is dominant in the tip-enhanced local field[30], the Raman polarizations are also induced along the *z*-direction. For effective coupling of incident fields and the local fields, the tip has to be in a position where the incident electric field in the *z*-direction is strong[12].

Figure 3 shows a typical experimental configuration for near-field Raman spectroscopy using a metallic probe. A silicon cantilever coated with a 40nm-thick silver layer by a thermal evaporation process is used as a metallic probe (Figure 4). A light field from a visible cw laser, *e.g.* a frequency-doubled $Nd:YVO_4$ laser (wavelength : 532 nm), enters into an epi-illumination optics after being expanded and collimated, and then focused onto a sample surface by using an oil-immersion objective lens (60x, NA=1.4). By bringing the silver-coated tip towards the focal spot, a strong optical field is generated to excite Raman scattering in the local volume between the tip apex and the substrate. The Raman signal is collected by the same objective lens and detected with a spectrometer equipped with
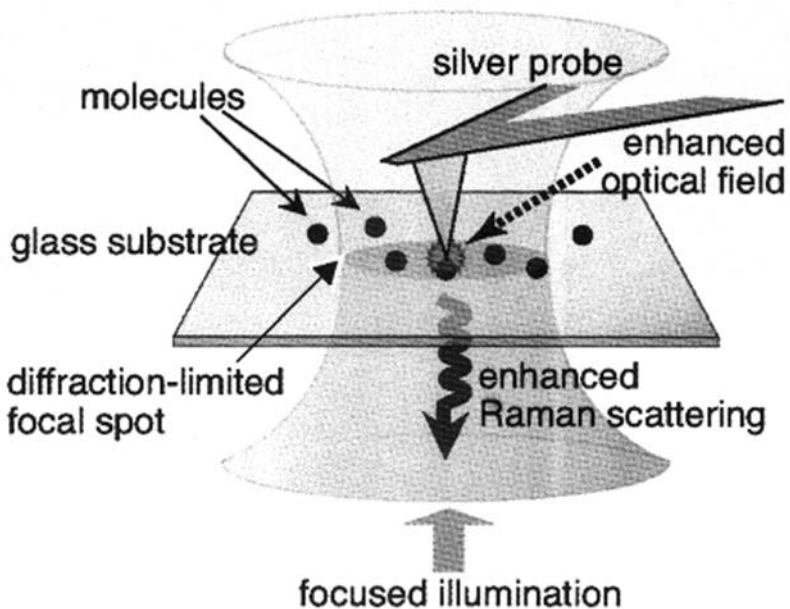

Fig. 2. A schematic of the local enhancement of Raman scattering by a silver probe tip in a tightly focused spot.
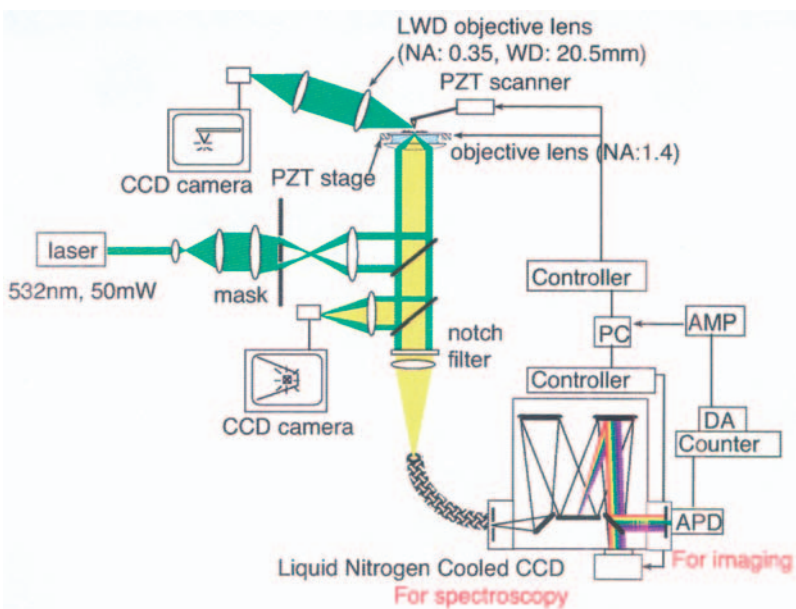
Fig. 3. *Optical setup for the tip-enhanced near field Raman spectroscopy using a metallic tip. See the text for detail.*

a liquid-nitrogen-cooled charge-coupled devices (CCD) detector for Raman spectrum measurement[5,7,9] and with an avalanche photodiode (APD) for Raman imaging[8]. Before the spectrometer, a holographic notch filter is placed to completely reject the excitation light. The
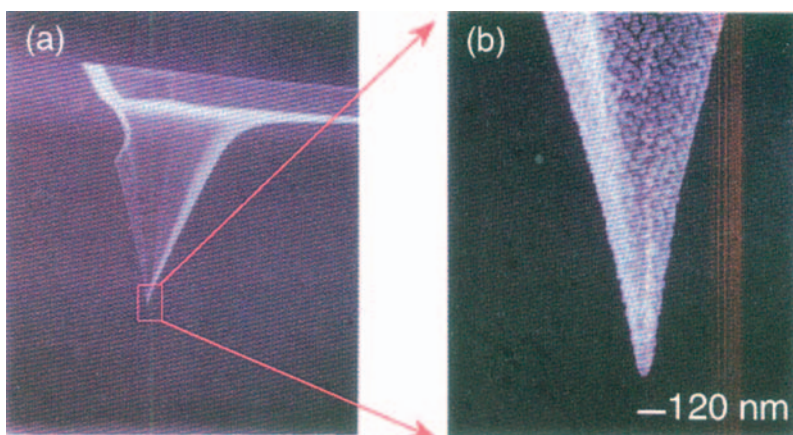

Fig. 4. *Scanning electron micrograph images of the tip apex of the silver-coated probe. The diameter of the tip apex is around 30 nm. (a) A complete image of the tip. (b) An expanded image of the tip apex.*

sample is scanned with piezoelectric transducers in the x-y plane, while the motion of the tip in the *z*-direction is controlled via an atomic force microscope (AFM) feedback system. For reduction of far-field background and stray light, part of the illumination light which corresponds to NA < 1.0 is rejected by inserting a mask in front of the beam splitter. The focused light spot consists only of the evanescent field, because only the component of the illumination light which corresponds to NA > 1.0 is transmitted through the mask.

Figure 5(a) shows a tip-enhanced Raman spectrum of adenine nanocrystals, one of the DNA bases, cast on a glass substrate. The Raman spectrum was measured when the tip was near the sample surface. Eight Raman bands, including two intense scattered bands at 739 and 1328 cm^{-1} due to the ring-breathing mode of whole molecule and the ring-stretching mode of diazole, respectively, were detected. The peak at 923 cm^{-1} was due to the Raman scattering of the glass substrate. As seen in Figure 5(b), a far-field Raman spectrum of the same sample, which was detected by using the same micro-
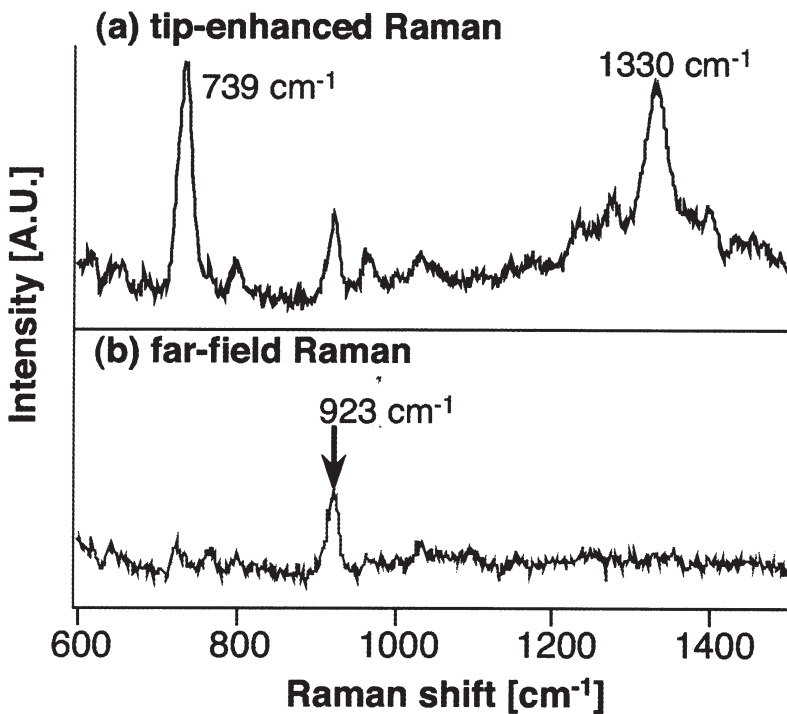

(a) tip-enhanced Raman
739 cm^{-1} 1330 cm^{-1}

(b) far-field Raman
923 cm^{-1}

Intensity [A.U.]

Raman shift [cm^{-1}]

600   800   1000   1200   1400

Fig. 5. *(a) A tip-enhanced near-field Raman spectrum of adenine enhanced by a metallized probe tip and (b) a far-field Raman spectrum.*

scope, when the tip was far away from the sample, shows almost no Raman scattering from the adenine nanocrystals except for the faint band at 723 cm^{-1}. The measurement conditions were exactly the same for both experiments except for the tip-sample distance. Exposure time was set to 1 min for both measurements.

Figure 6(a) shows a spectral mapping of the tip-enhanced Raman spectra for the adenine nanocrystals, obtained using the silver-coated tip at 30-nm intervals with the AFM contact mode[11]. The exposure time of the image was set to 10 s per scan. Figure 6(b) exhibits intensity distributions of the two predominant Raman bands at 739 and 1328 cm^{-1}. The intensity distribution at 850 cm^{-1}, where no Raman band exists, shows no particular optical response signal in the same figure. The peak response at 60 nm of the *x*-axis as well as the edge response of the intensity profile around 120 nm of the *x*-axis in Figure 6(b) suggests that the smallest feature of the spatial distribution of adenine molecules is 30 nm in this experiment. Assuming that the diameter of the enhanced electric field is 30 nm corresponding to the diameter of the lateral resolution and that the diameter of the focused light spot is 400 nm, the enhancement factor for the ring-breathing mode of the whole molecule at 739 cm^{-1} is 2.7×10^3. Furthermore, it is difficult to calculate the enhancement factor for the band at 1328 cm^{-1} because the far-field Raman signal without the tip is too weak to be detected. An enhancement factor of 10^3–10^4 observed with a silver-coated tip is reasonable compared to the SERS spectra of adenine nanocrystals adsorbed on silver spheres having the same radii as the width of the probe tip apex (the excitation frequency is also the same).

Other DNA bases, thymine, guanine, and cytosine have their specific Raman bands due to the ring-breathing modes at 670, 681, 782 cm^{-1}, respectively[31]. A whole DNA sequence can be identified directly by detecting such specific ring-breathing modes by the tip-enhanced near-field Raman spectroscopy without dye-staining as compared to ordinary DNA sequencing methods such as fluorescence *in situ* hybridization (FISH), where the spatial resolution is restricted by the diffraction limit.

The tip-enhanced Raman spectroscopy has also been applied to analyze the local vibrational modes of individual SWNTs[9]. Raman spectroscopy has been recently recognized as a very powerful tool for the measurements of SWNTs because much structural information on the chirality and diameter can be deduced from the vibration spectra[32–34]. To understand further detail of the specific structure-dependent 'single molecule' property, a single-molecule addressing capability at nanometer scale is needed, which is now provided by
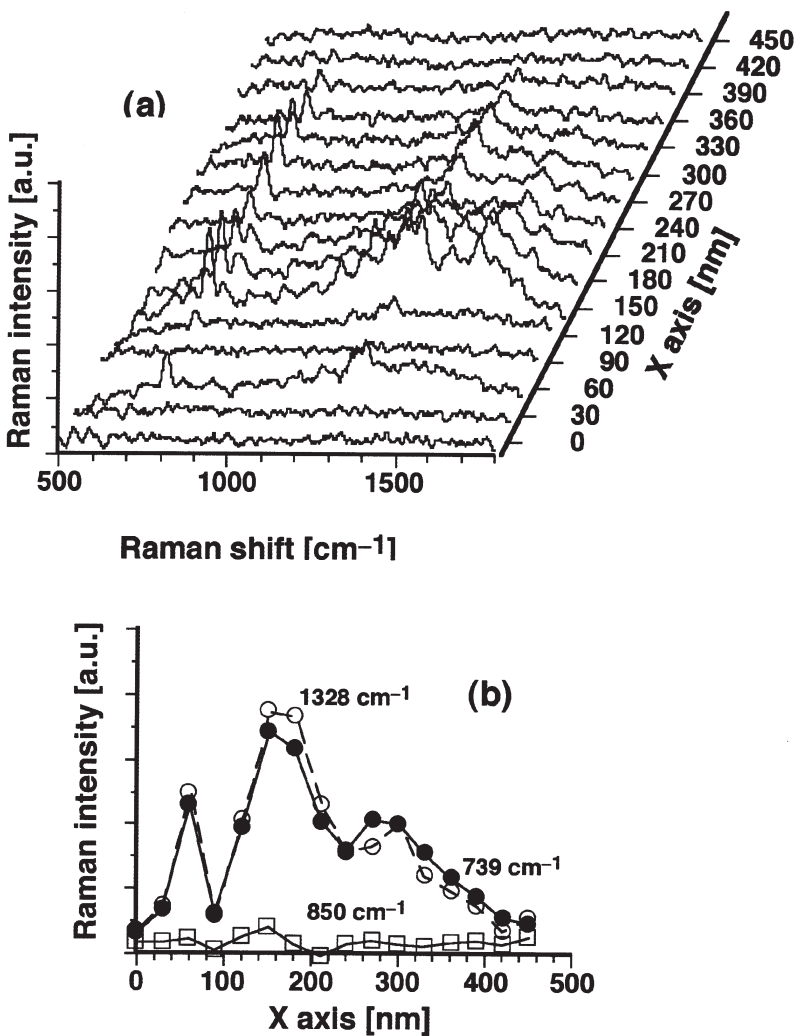
Fig. 6. *(a) Tip-enhanced near-field Raman spectral mapping of adenine nano-crystals at 30 nm intervals. Each spectrum is the subtraction of the corresponding tip-enhanced near-field Raman spectrum from the far-field Raman spectrum. (b) Raman intensity distributions of the Raman bands at 739 and 1328 cm^{-1} against the tip displacement within the focused spot. The intensity distribution at 850 cm^{-1} is also given for a comparison.*

the tip-enhanced near-field microscopy. For these measurements, SWNTs were spread out on a glass substrate, and a laser beam with 532 nm wavelength was focused at a tube.

Figure 7 shows a tip-enhanced near-field Raman spectrum of an individual SWNT, obtained schematically at the probe position 'A'. Remarkable tangential G-band peaks, representing graphite mode of a SWNT, that is split into three peaks and fitted well to the Lorentzian line shape at 1593, 1570, and 1558 cm^{-1}, were observed
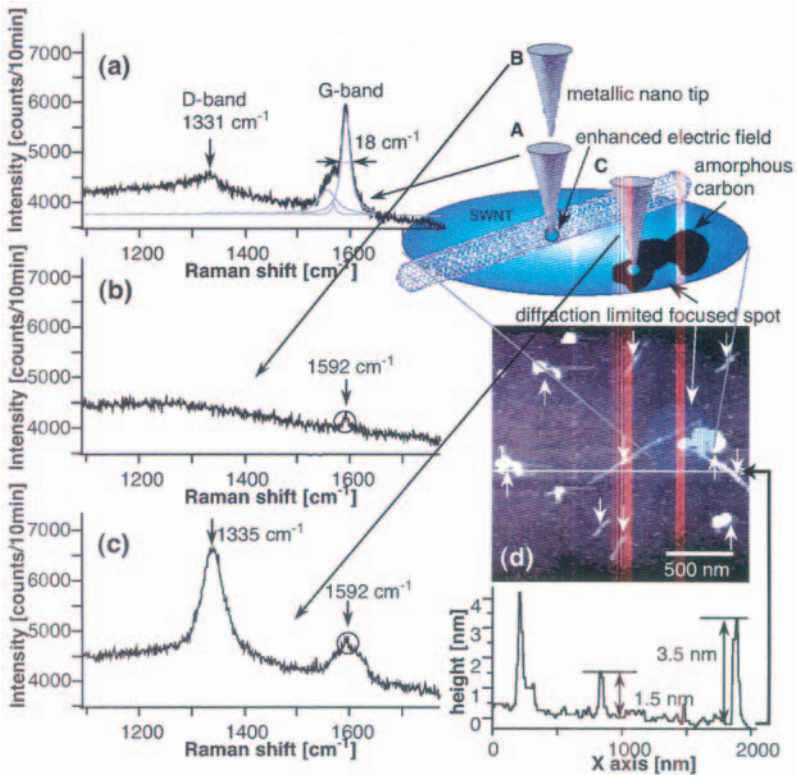

Fig. 7. *(a) A tip-enhanced near-field Raman spectrum of an individual SWNT, which was obtained at the tip position 'A' shown schematically. (b) A far-field Raman spectrum of SWNT including impurities (amorphous carbon) when the tip was 500 nm away from the sample surface, schematically shown in 'B'. (c) A tip-enhanced near-field Raman spectrum of amorphous carbon, which is obtained at the probe position 'C' shown schematically in the figure. (d) A topographic atomic force microscope image and the cross-section (white line in the image indicated by a solid arrow) of the isolated SWNTs dispersed on a glass substrate. The far-field focused spot is indicated by the mask grid pattern in the image. Some isolated SWNTs indicated by downwards arrows and amorphous carbon particles indicated by upwards arrows can be seen in the image. The dimension of the image is 2 mm $\times$ 2 mm consisting of 200 $\times$ 200 pixels.*

(gray lines in Figure 7(a)). These Lorentzian line shapes feature semiconductive SWNTs. While the fitted linewidth at 1593 cm^{-1} is 18 cm^{-1}, the actual line width is deduced to be 8 cm^{-1} by considering the slit width of the spectrometer. This narrow linewidth supports that the observed isolated SWNTs consist of only one or a few SWNTs [35]. A small D-band peak, representing defect mode, at 1331 cm^{-1} was also detected.

Figure 7(b) was obtained when the metallic probe tip was 500 nm away from the sample surface (the tip position 'B'). This spectrum represents a far-field Raman spectrum, where the featured lines vanished due to the absence of field enhancing metallic probe tip, except a small protrusion at 1592 cm^{-1}. Since the sample contains not only SWNTs but also impurities (amorphous carbon), this small peak represents an average within the focused spot of laser beam. The peak seen in Figure 7(b), however, dominantly reflects G-band feature of SWNTs. Figure 7(c) shows another tip-enhanced near-field Raman spectrum from the same sample when the probe enhanced field at a different location 'C'. A broad D-band representing defect mode of amorphous carbon was dominantly detected around 1335 cm^{-1}. G-band is also seen but wider than that seen in Figure 7(a). A small G-band peak shown in Figure 7(b) (circle in the figure) is recognizable on the top of the broad G-band peak in Figure 7(c) (circle in the figure). The broad G-band peak represents the tip-enhanced near-field Raman scattering of amorphous carbon, while the small G-band peak is the far-field background signal coming from an isolated SWNT.

Raman spectroscopy can also provide information on the diameter of SWNTs. Radial breathing mode observed in the lower frequency region strongly relates to the diameter of the SWNTs. Figures 8(a), (b) and (c) show tip-enhanced near-field, far-field, and the subtracted Raman spectra, respectively. The metallic probe tip selectively enhanced the SWNT just below the tip so that the enhanced Raman peak at 165.2 cm^{-1} was clearly observed in Figure 8(a) while other peaks such as 170.8 cm^{-1} and 192.6 cm^{-1} which were generated from the far-field focused spot were not enhanced. By using a widely-used approximation for individual SWNTs, $\omega_{RBM} = 248/d$ (ω_{RBM}: frequency of the ring-breathing mode, d: diameter of the SWNT) [32], the Raman peak at 165.2 cm^{-1} corresponds to a diameter of 1.50 nm. A topographic image of the sample (Figure 7(d)) agrees with the height of the SWNT (~ 1.5 nm) and clearly shows the distribution of SWNTs and amorphous carbon. White lines in the figure indicated by downwards arrows are isolated SWNTs. The other isolated SWNT has the height of 3.5 nm consisting of several SWNTs in the cross sectional line profile. From the estimated diameter of the
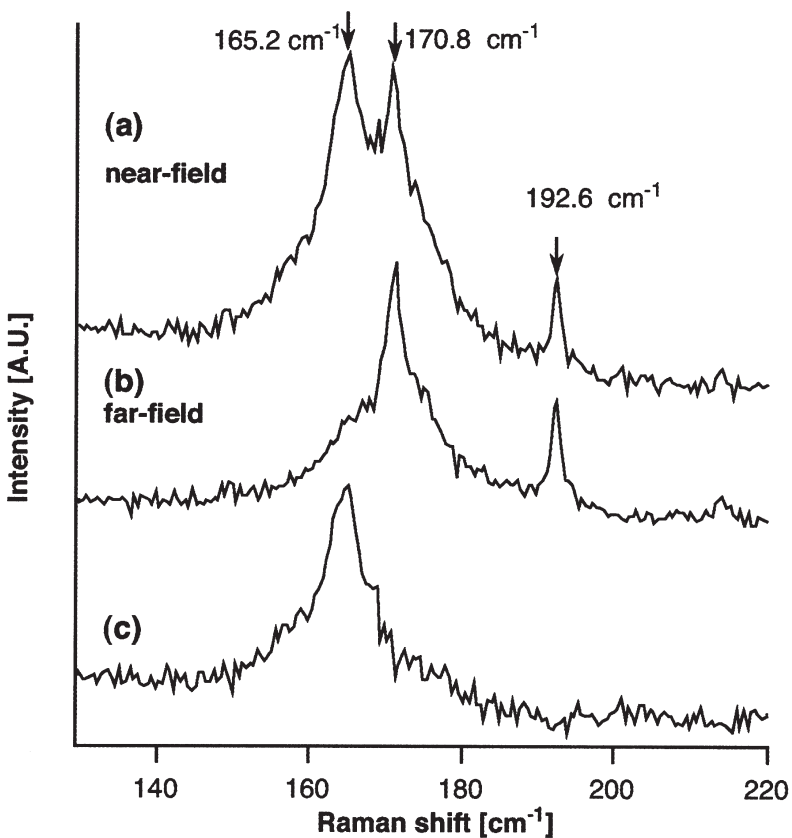
Fig. 8. (a) A tip-enhanced near-field and (b) a far-field Raman spectra of radial breathing mode of isolated SWNTs. (c) is the subtraction of the spectrum in (b) from the spectrum in (a). The Raman peak at 165.2 cm⁻¹ corresponding to the diameter of 1.50 nm is selectively enhanced by the metallic probe tip. The laser power is 4.8 mW and the exposure time is 1 minute.

SWNT and semiconductive feature found in the spectral shape of the G-band, accordingly, the most possible chirality for the semiconductive SWNT observed in the tip-enhanced Raman spectrum has been estimated to be (17.4) with a diameter of about 1.513 nm.

4. Tip pressurized Raman Spectroscopy

The well-known SERS effect is contributed not only by the electromagnetic enhancement but also chemical enhancement effect. The chemical effect can be explained as charge transfer in the chemical complex consisting of the metal atom and the adsorbed molecule[36–38].

The chemical effect involves spectral shifts of Raman spectra of the adsorbed molecules besides the amplification of the Raman signals. The same effect can be observed in the tip enhancement of Raman scattering, in which the silver on the probe tip also chemically interacts with the sample and hence causes a spectral shift. Furthermore, when a tip is in contact with the molecules based on the feedback scheme of atomic force microscopy, the tip mechanically pressurizes the molecules and distorts the molecular orbits. This leads to another spectral shift with respect to the conventional SERS spectrum[11].

Figure 9 represents the spectral difference amongst (a) tip-enhanced near-field Raman scattering, (b) SERS, and (c) conventional near-infrared Raman scattering. It is seen that the band due to the ring-breathing mode at 739 cm^{-1} in the near-field Raman spectrum (Figure 9(a)) is 16 cm^{-1} higher than the Raman band of the ring-breathing mode in the normal Raman spectrum (Figure 9(c)). The band due to the same mode in the SERS spectrum is at 733 cm^{-1}, which is only 10 cm^{-1} higher than that in the Raman band of the ring-breathing mode in the normal Raman spectrum. Although the SERS spectrum of adenine molecules depends on the substrate used[36,39], the large band shift found in the tip-enhanced Raman spectrum cannot be explained as the substrate effect. This interesting phenomenon suggests that the shifts of Raman frequencies caused by dynamic contact of the silver-coated tip on the samples may differ from the shifts attributed to the surface enhancement effects caused by thermally stable adsorption of the samples onto the silver surfaces in the conventional SERS.

In order to analyze the frequency shifts of Raman bands of adenine affected by the silver-coated tip, the vibrational frequencies of the Raman intensities have been calculated using density-functional theory (DFT) calculations[40-42] for adenine and its silver complexes. Several possible adenine-silver complex isomers were examined in which the silver atom at the tip is adjacent to any nitrogen atoms. Comparing the calculated Raman spectra with the SERS spectrum of Figure 9(b), a silver-adenine complex shown in Figure 10, in which the silver atom is adjacent to the N3 atom, is found to best represent the SERS spectrum. Although whole spectral patterns of the calculated Raman spectrum of the model are similar to that of the tip-enhanced near-field Raman spectrum, the large frequency shift of the tip-enhanced near-field Raman band towards high frequency due to the ring-breathing mode at 739 cm^{-1} does not appear in the calculated spectrum.

The major difference in experimental conditions of the tip-enhanced Raman detection from those of the SERS spectroscopy is
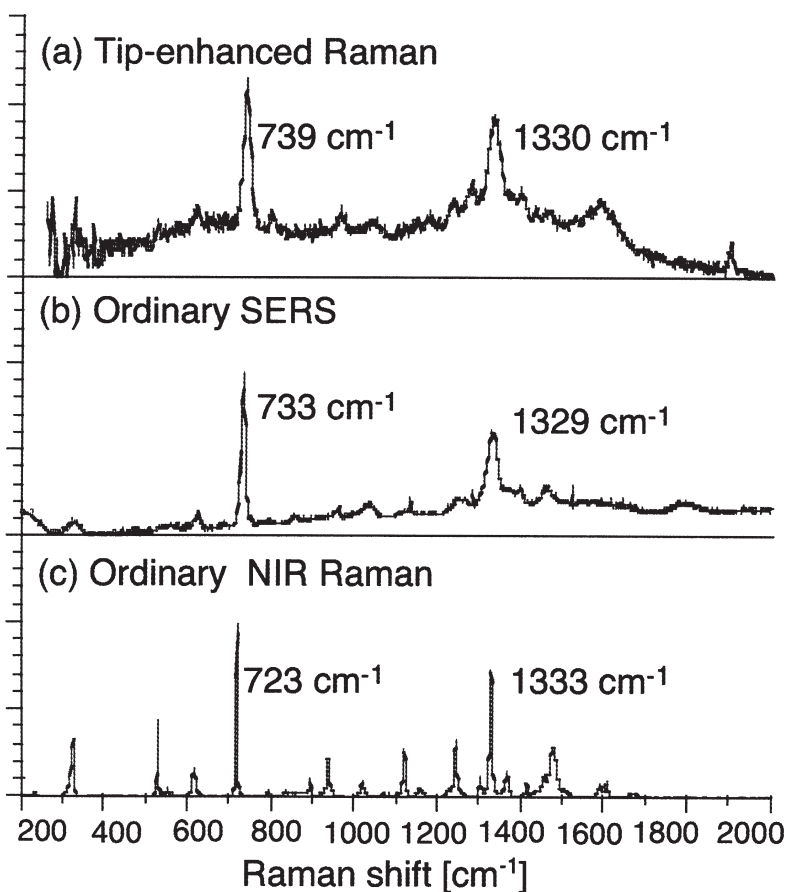
Fig. 9. *Spectral difference amongst (a) the tip-enhanced Raman, (b) the ordinary SERS, and (c) ordinary near-infrared (NIR) Raman spectra. In the tip-enhanced Raman detection, a single nano-crystal (7 nm × 30 nm × 7 nm) of adenine was observed with an exposure time of 1 min. In the SERS detection, a silver island film (1 mm × 1 mm × 100 nm) was used to enhance the Raman signal of adenine with an exposure time of 1 min. The NIR Raman detection used a thick sample of adenine (1 mm × 1 mm × 100 μm) with a 1 hour exposure. Since a different spectrometer with a higher spectral resolution was used in the NIR Raman measurements, the spectral widths in (c) are smaller than those in (a) and (b).*

the interaction mechanism of adenine with silver surfaces. In SERS, adenine is adsorbed in equilibrium onto silver surfaces, whereas in the tip enhancement nano-crystalline adenine is pressed by the silver probe tip with a constant atomic force. Assuming that the atomic force is applied only to the contraction of the bond between the
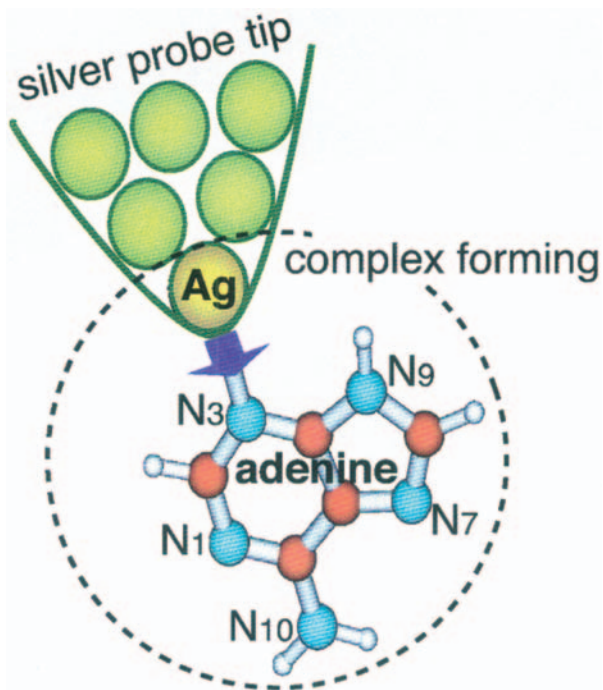
Fig. 10. *Deduced geometry of silver-adenine complex. The silver atom is adjacent to the N_3 nitrogen atom.*

silver atom of the tip and the adjacent nitrogen of the adenine molecule, the bond distance would be expected to shrink and the vibrational frequencies may then shift. In the tip-enhanced Raman detection, a cantilever with a spring constant of 0.03 N/m was used and a silver-coated tip apex diameter of this cantilever was 5 ~ 10 nm. The atomic force was kept constant at 0.3 nN by the feedback loop. Deduced from the unit cell parameters of single crystal 9-methyl-adenine[43], a couple of adenine molecules exist within a rectangle area of 0.77 nm by 0.85 nm. If we assume that the force is equally applied to all the molecules which are adjacent to the tip apex, the adenine molecules are subjected to a pressure of *ca* 1–5 pN/molecule by the silver atom attached on the surface of the tip. For the further understanding of the tip-enhanced near-field Raman active species of adenine molecules, we investigated the transition states of the silver-adenine complex by changing the bond distance (in the model) between the nitrogen of adenine molecule and the silver atom. In the calculations, the bond distance was set to 2.502 (equilibrium), 2.75 (10% elongation), 2.25 (10% contraction), and 2.0 angstroms (20%

contraction). The calculated frequency shifts of the two major Raman bands having high intensities in the tip-enhanced Raman spectroscopy and the calculated potential curves are plotted as a function of the bond distance in Figure 11.

As the metallic tip of the cantilever approaches the surface of adenine nano-crystal, the tip is subject to the van der Waals attractive force at first and after passing through the equilibrium point, the tip receives a repulsive force. In the experiment, the atomic force which is balanced with the repulsive force is set at 1–5 pN/molecule as described before. When the bond distance of the AgN linkage is reduced by 10%, the repulsive force of 7 pN/molecule is derived from a harmonic oscillation of the displacement by 0.025 nm and the energy difference by 1.7 kcal/mol. The repulsive force coincides with the atomic force obtained with the AFM system.

The ring-breathing mode shows a significant shift towards a higher frequency as a function of the contracted bond distance between the silver atom and the N_3 nitrogen of adenine (Fig. 11(b)). The frequency of the ring-breathing mode is shifted upwards by 5 cm^{-1} when the bond distance is reduced by 10%. The frequency is shifted upwards by 17 cm^{-1} when the bond distance is reduced by 20%. In contrast, the calculated frequency shift of the other band (Figure 11(a)) is very small. The frequency shifts of these two bands agree with those of the bands seen in the experiments.

It is concluded that the near-field effects in the tip-enhanced Raman scattering can be classified into three effects: (1) the electromagnetic effect due to the local surface plasmon resonance in the nano-scaled metallic tip; (2) the chemical effect due to the chemical complex and charge transfer between the adsorbed molecules and the metal; and (3) the mechanical effect due to the distortion of molecular orbital caused by the tip pressurization. Since the latter two effects are sensitive to molecules directly attached to the silver atom on the tip end, they may give possibility to bring the spatial resolution of tip-enhanced Raman spectroscopy down to the molecular scale.

5. Tip-enhanced CARS spectroscopy: combination with nonlinear Raman scattering

High-order nonlinear optical phenomena are alternatives to confine photons in a smaller volume than the size of the diffraction-limited focal spot. The probability of the nonlinear effects is proportional to the high-order powers of the incident light intensity. In the case of two-photon-excited fluorescence, for which the probability is
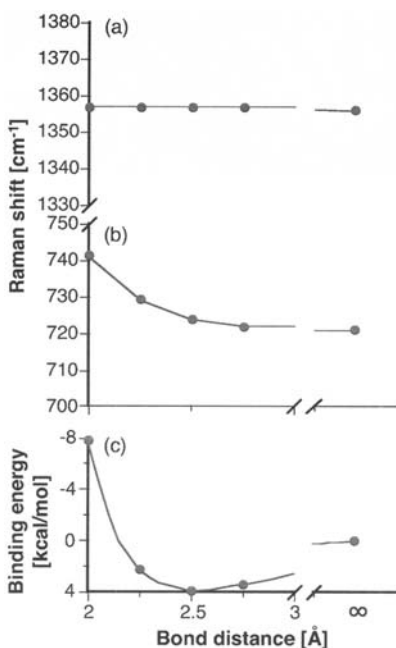
Fig. 11. *(a), (b) The calculated frequency shifts of two Raman bands of the silver-adenine complex shown in Fig. 10, respectively. (c) The calculated binding energies as a function of the bond length for the AgN linkage.*

quadratically proportional to the excitation intensity, in a diffraction limited focal spot, the spatial distribution of the fluorescence emission becomes narrower than the intensity distribution of the excitation field. This leads to the reduction of the effective volume of light-matter interaction beyond the diffraction limit. Higher-order optical effects give much finer spatial response (Figure 12(a)). So far, many types of microscopic and fabrication methods using nonlinear optical effects have been reported[44,45].

The tip-enhanced near-field microscopy can also benefit from the high order nonlinear effects. The volume of the light-matter inter-action can be further confined to the tiny portion at the very end of the metallic tip. Because of the nonlinear responses, even a small enhancement of the excitation field could lead to a huge enhance-ment of the emitted signal, allowing a relative reduction of the far-field background.

In order to realize tip-enhanced nonlinear molecular-vibration spectroscopy, coherent anti-Stokes Raman scattering (CARS) spectroscopy is employed, which is the most widely used nonlinear Raman spectroscopy [46]. The CARS spectroscopy uses three incident
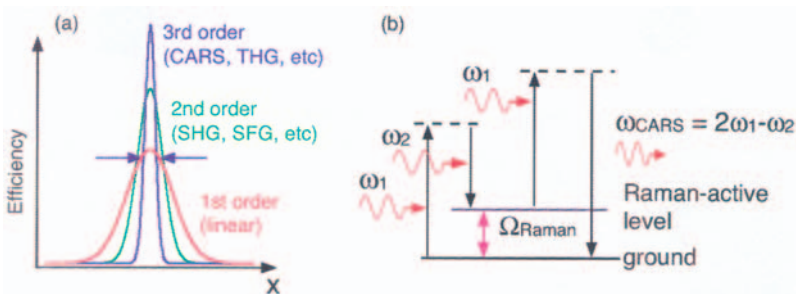
Fig. 12. *(a) Improvement of spatial resolution and signal enhancement in the nonlinear optical effect. (b) Energy diagram of coherent anti-Stokes Raman scattering (CARS) process.*

fields including a pump field (ω_1), a Stokes field (ω_2; $\omega_2 < \omega_1$), and a probe field ($\omega_1' = \omega_1$), and induces a nonlinear polarization at the frequency of $\omega_{CARS} = 2\omega_1 - \omega_2$, as shown in Fig. 12(b). When the frequency difference of ω_1 and ω_2 ($\omega_1 - \omega_2$) coincides with one of the specific molecular vibrational frequencies (Ω) of Raman-active modes of a given sample, the anti-Stokes Raman signal is resonantly generated. Recently, several scientists have reported that a tight focusing of the excitation field with a high NA objective lens can bring CARS microscopy to a three-dimensional imaging capability at a submicron scale[47,48]. The phase matching condition can be automatically satisfied in the focused fields of any angles[49]. In other words, it is not necessary to consider the phase matching condition when the CARS polarizations are generated only in a volume smaller than the propagation wavelength of the CARS field[50]. Surface enhanced CARS was also reported, in which CARS was amplified by isolated gold nanoparticles[51,52]. These reports verified the possibility of the local enhancement of CARS by a metallic nano-structure. Based on the concept mentioned above, one can observe CARS signals generated by the enhanced electric field at a metallic tip end of nanometric scale.

Figure 13 shows the experimental system of the tip-enhanced CARS microscopy[12,13,53]. As similar to the tip-enhanced normal Raman spectroscopy, the system mainly consists of an excitation laser, an inverted microscope, an atomic force microscope using a silver-coated probe, and a monochromator. Two mode-locked Ti:sapphire lasers (pulse duration: 5 ps, spectral band width: 4 cm^{-1}, repetition rate: 80 MHz) are used for the excitation of CARS. The ω_1 and ω_2 beams are collinearly overlapped in time and space, and introduced into the microscope with an oil-immersion objective lens (NA = 1.4) focused onto the sample surface. The repetition rate of
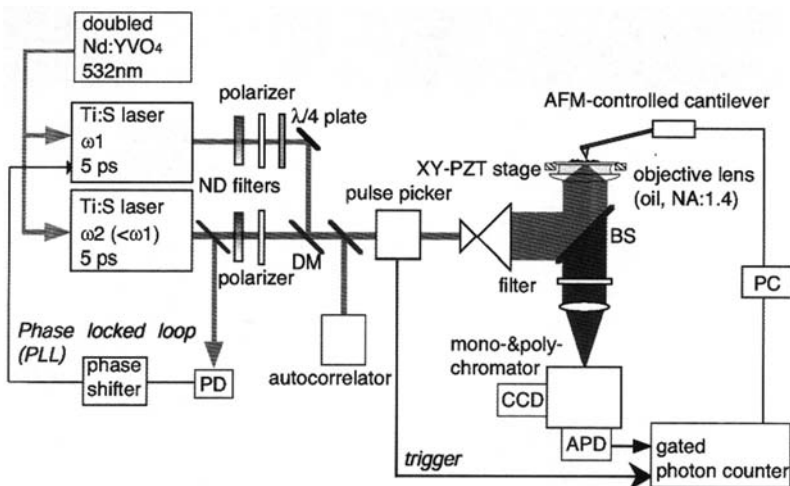
Fig. 13. *Experimental setup for the tip-enhanced CARS microscopy. See the text for detail.*

the excitation lasers is controlled by an electro-optically (EO) modulated pulse picker. The backscattered CARS emission enhanced by the probe tip is collected with the objective lens and detected with an APD based photon-counting module through an excitation-cut filter and the monochromator. The observing spectral width through the detection system is about 12 cm^{-1}. The pulse signal from the APD are counted by a time-gated photon counter synchronously triggered with the pulse picker, which effectively reduces the dark counts down to almost 0 counts/sec.

The DNA molecules of poly(dA–dT) aggregated into clusters were used as a model sample for CARS imaging. The poly(dA–dT) solution in water (250 μg/ml) was cast and dried on a glass substrate at the room temperature with the fixation time of ~24 hours. The dimensions of the clusters are typically 20 nm in height and 100 nm in width. The frequency difference of the two excitation lasers for CARS imaging was set to 1337 cm^{-1}, corresponding to a Raman mode of adenine (ring-stretching mode of diazole), by tuning the excitation frequencies ω_1 and ω_2 to be 12710 cm^{-1} (λ_1: 786.77 nm) and 11373 cm^{-1} (λ_2: 879.25 nm), respectively. After the imaging in this resonant condition, the frequency of ω_2 was changed such that the frequency difference corresponds to none of the Raman-active vibrations.

Figure 14 shows the CARS images of the DNA clusters obtained by our system. Figures 14(a) and (b) are the tip-enhanced CARS image in the on-resonant condition (ω_1-ω_2 = 1337 cm^{-1}) and the
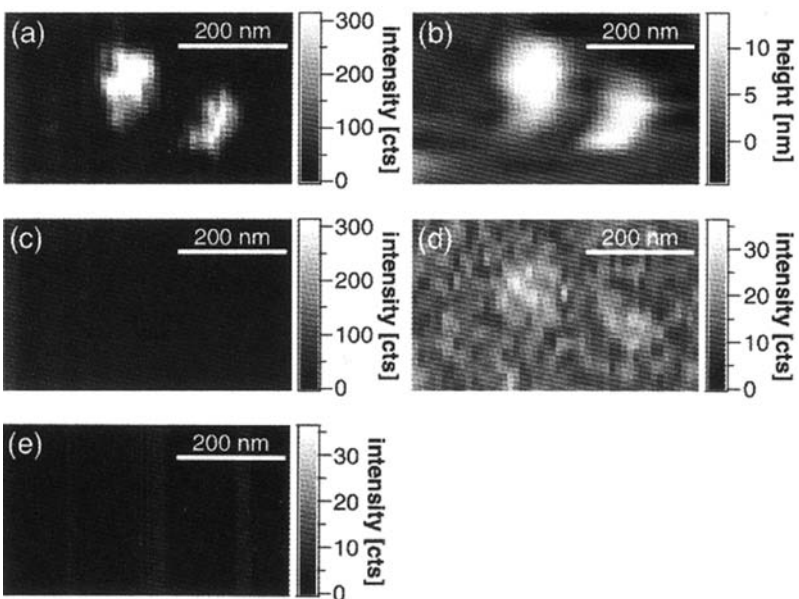
Fig. 14. *CARS images of the DNA clusters. (a) A tip-enhanced CARS image in the on-resonant condition ($\omega_1-\omega_2 = 1337$ cm^{-1}), and (b) the simultaneously obtained topographic image. (c) Tip-enhanced CARS image in the off-resonant condition ($\omega_1-\omega_2 = 1278$ cm^{-1}). (d) The same image as (c) shown with a different gray scale. (e) A CARS image of the same area as in (a), obtained without the silver tip. The scanned area is 500 nm by 300 nm. The pixel dwell time was 100 ms, and the acquisition time for obtaining one image was about 3 minutes. The average powers of the ω_1 and ω_2 beams were 30 μW and 15 μW, respectively, at the 800 kHz repetition rate.*

simultaneously acquired topographic AFM image, respectively. The DNA clusters of about 100 nm diameter are visualized in Figure 14(a). The two DNA clusters with separation of about 160 nm are clearly distinguished by the tip-enhanced CARS imaging. This indicates that the CARS imaging can successfully achieve the super-resolving capability beyond the diffraction limit of light. In the off-resonant condition ($\omega_1-\omega_2 = 1278$ cm^{-1}), the CARS signals mostly vanish in Figure 14(c). Figures 14(a) and (c) verify that vibrationally resonant CARS is emitted from the DNA molecules at a specific frequency. However, a slight trace of the clusters could be seen in the off-resonant condition in Figure 14(d), which is the same as Figure 14(c) but is shown with a different gray scale. This can be caused by both the frequency-invariant (non-resonant) component of the non-linear susceptibility of DNA [46] and the topographic artifact[54].

Figure 14(e) is a CARS image at the on-resonant frequency which was obtained after removing the tip from the sample. The CARS signal was not detected in the CARS image without the silver tip, which confirms that the CARS polarization in Figure 14(a) was effectively induced by the tip-enhanced field. The background signal seen in the Figure 14(d) is attributed to both local four-wave-mixing (FWM) emission of silver probe due to its nonlinear susceptibility and white light continuum (WLC) of silver due to the electron-hole recombination[55,56]. These two components compete with the CARS process and degrade the image contrast and signal-to-noise ratio. Further, they subsequently limit the smallest number of molecules that can be observed. In this experiment, however, the tip-enhanced CARS signal intensity largely surpasses the background because the number of molecules in the excited volume was enough to induce the signal.

In order to assess the spatial resolution and the capability of the sensitivity of the tip-enhanced CARS microscopy, a DNA network of poly(dA–dT)-poly(dA–dT) was prepared[57]. The DNA (poly(dA–dT)-poly(dA–dT)) dissolved in water (250 µg/ml) was mixed with $MgCl_2$ (0.5 mM) solution, then the DNA solution was cast on a glass substrate and blow-dried after the fixation time of 2 hours. Mg^{2+} has a role for the linkage between DNA and oxygen atoms of the glass surface. Figure 15(a) shows a typical topographic image of the DNA network sample. The DNA network consists of bundles of DNA double-helix filaments aligned parallel on the glass substrate. Since the diameter of single DNA double-helix filaments is about 2.5 nm, the height of the bundle structures is about 2.5 nm, and the width is from 2.5 nm (for single filaments) to a few tens of nanometers (for *ca* 10 filaments). The CARS images at the on- and off-resonant frequencies are shown in Figures 15(b) and (c). The DNA bundles were observed at the resonant frequency shown in Figure 15(b), while they could not be visualized at the off-resonant frequency in Figure 15(c). This indicates that the observed contrast is dominated by the vibrationally resonant CARS signals. Figure 15(d) shows the one-dimensional profiles of the row indicated by solid arrows, which were acquired with a 5 nm step. The line profile acquired without the silver tip is also added for comparison. Only the CARS profile with the tip in the on-resonant condition has peaks at the positions of x ~ 370 nm and x ~ 700nm, where adenine molecules exist in the DNA double helix, while the other line profiles do not sense the existence of the molecules. The full width of half maximum of the right peak is found to be about 15 nm, as indicated in Figure 15(d).

The size of the locally excited volume of the DNA structure is estimated to be about 1 zeptolitre[58]. The intensity enhancement factor
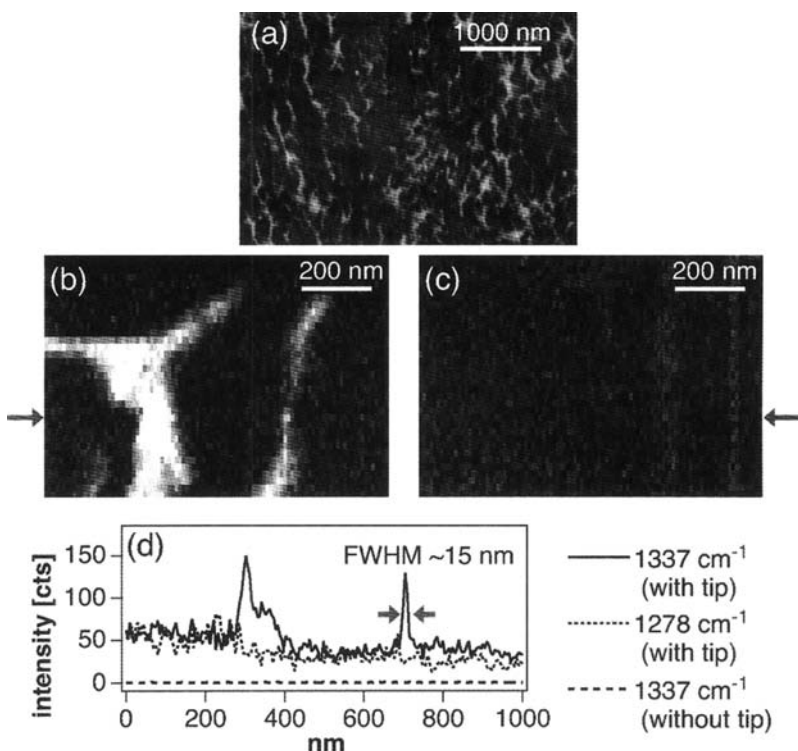
Fig. 15. *CARS images of the DNA network. (a) A topographic image of the DNA network. (b) A tip-enhanced CARS image in the on-resonant condition ($\omega_1-\omega_2 = 1337$ cm^{-1}). (c) A tip-enhanced CARS image in the off-resonant condition ($\omega_1-\omega_2 = 1278$ cm^{-1}). (d) One-dimensional line profiles at the positions indicated by the solid arrows. The scanned area is 1000 nm by 800 nm. The pixel dwell time was 100 ms, and the acquisition time for obtaining one image was about 12 minutes. The average powers of the ω_1 and ω_2 beams were 45 μW and 23 μW, respectively, at the 800 kHz repetition rate.*

of the CARS intensity is also estimated to be of the order of 10^6.[59]. The estimated enhancement factor for the CARS intensity (10^6) leads to the enhancement factor of the order of 100 for each excitation field. This factor is quite realistic and reasonable, as compared to the previous numerical results[17–20], although this estimation is very much subject to the changes in each parameter with high-order dependency. The smallest detectable volume of DNA under the current experimental condition is estimated to be as small as 1/4 zeptolitre, which is derived from the signal-to-noise ratio of about 15 in Figure 15(d) and the quadratic dependence of the CARS intensity

on interaction volume. This indicates that our CARS microscope is capable of sensing a vibrational-spectroscopic signal from an enormously small subzeptolitre volume.

6. Conclusions

The application of near-field optics to Raman spectroscopy opens up the gates to nanospectroscopy and nanoanalysis. Attractive nanomaterials such as nanocarbons (SWNT, C_{60}, *etc*.) and biomolecules (DNA, protein, *etc*.), which have been in the spotlight of science, can be observed and evaluated on the nanometric scale using tip-enhanced Raman spectroscopy. The technique provides colored images composed of plentiful information of molecular species, without the need for dye staining. It would greatly contribute to the advances of nanotechnology and nanosciences. The recent reports on the combination with tip-pressurization analysis and nonlinear Raman spectroscopy have made meaningful steps toward the realization of the molecular-scale spatial resolution and sensitivity.

References

1 Pohl, D. W., Denk, W. and Lanz, M. (1984) *Appl. Phys. Lett.*, 44, 651.
2 Betzig, E., Trautman, J. K., Harris, T. D., Weiner, J. S. and Kostelak, R. L. (1991) *Science*, **251**, 1468.
3 Betzig, E., and Chichester, R. J. (1993) *Science,* **262**, 1422.
4 Inouye, Y. and Kawata, S. (1994) *Opt. Lett*., **19**, 159.
5 Inouye, Y., Hayazawa, N., Hayashi, K., Sekkat, Z. and Kawata, S. (1999) *Proc. SPIE*, **1791**, 40.
6 Stöckle, R. M., Suh, Y. D., Deckert, V. and Zenobi, R. (2000) *Chem. Phys. Lett*., **318**, 131.
7 Hayazawa, N., Inouye, Y., Sekkat, Z. and Kawata, S. (2000) *Opt. Commun*., **183**, 333.
8 Hayazawa, N., Inouye, Y., Sekkat, Z. and Kawata, S. (2002) *J. Chem. Phys.*, **117**, 1296.
9 Hayazawa, N., Yano, T., Watanabe, H., Inouye, Y. and Kawata, S. (2003) *Chem. Phys. Lett.*, **376**, 174.
10 Hartschuh, A., Sanchez, E. J., Xie, X. S. and Novotny, L. (2003) *Phys. Rev. Lett.*, **90**, 95503.
11 Watanabe, H, Ishida, Y., Hayazawa, N., Inouye, Y. and Kawata, S. (2004) *Phys. Rev.*, **B69**, 155418.
12 Hayazawa, N., Ichimura, T., Hashimoto, M., Inouye, Y. and Kawata, S. (2004) *J. Appl. Phys.*, **95**, 2676.
13 Ichimura, T., Hayazawa, N., Hashimoto, M., Inouye, Y. and Kawata, S. (2004) *Phys. Rev. Lett.*, **92**, 220801.
14 Wolf, E. and Nieto-Vesperinas, M. *J.* (1985) *Opt. Soc. Am.*, **A2**, 886.

15 Kawata, S. (ed.) (2001) *Near-Field Optics and Surface Plasmon Polaritons*, Springer, Berlin.

16 Kawata, Y., Xu, C. Xu, and Denk, W. (1999) *J. Appl. Phys.*, **85**, 1294.

17 Furukawa, H. and Kawata, S. (1998) *Opt. Commun.*, **148**, 221.

18 Kottmann, J. P., Martin, O. J. F., Smith, D. R. and Schultz, S. (2001) *J. Microsc.*, **202**, 60.

19 Martin, Y. C., Hamman, H. F. and Wickramasinghe, H. K. (2001) *J. Appl. Phys.*, **89**, 5774.

20 Krug, J. T, II, Sánchez, E. J. and Xie, X. S. (2002) *J. Chem. Phys.*, **116**, 10895.

21 Hayazawa, N., Inouye, Y. and Kawata, S. (1999) *J. Microsc.*, **194**, 472.

22 Hamman, H. F., Gallagher, A. and Nesbitt, D. J. (2000) *Appl. Phys. Lett.*, **76**,1953.

23 Sánchez, E. J., Novotony, L. and Xie, X. S. (1999) *Phys. Rev. Lett.*, **82**, 4014.

24 Lahrech, A., Bachelot, R., Gleyzes, P. and Boccara, A.C. (1996) *Opt. Lett.*, **21**, 1315.

25 Knoll, B. and Keilmann, F. (1999) *Nature*, **399**, 134.

26 Masaki, T., Goto, K., Inouye, Y.and Kawata, S. (2004) *J. Appl. Phys.*, 95, 334.

27 Chang, R. K. and Furtak, T. E. (1982) *Surface Enhancement Raman Scattering*, Plenum, New York.

28 Nie, S. and Emory, S. R. (1997) *Science*, **275**, 1102.

29 Kneipp, K., Wang, Y., Kneipp, H., Perelman, L. T., Itzkan, I., Dasari, R. R. and Feld, M. S. (1997) *Phys. Rev. Lett.*, **78**, 1667.

30 Novotny, L., Sanchez, E. J.and Xie, X. S. (1998) *Ultramicroscopy*, **71**, 21.

31 Deng, H., Bloomfield, V. A., Benevides, J. M. and Thomas, G. J., Jr. (1999) *Biopoly*, **50**, 656.

32 Jorio, A., Saito, R., Hafner, J. H., Lieber, C. M., Hunter, M., McClure, T., Dresselhaus, G. and Dresselhaus, M. S. *Phys. Rev. Lett.*, 86, 1118 (2001)

33 Duesberg, G. S., Loa, I., Burghard, M., Syassen, K. and Roth, S. (2000) *Phys. Rev. Lett.*, 85, 5436.

34 Dresselhaus, M. S. and Eklund, P. C. (2000) *Adv. Phys.*, **49**, 705.

35 Kneipp, K., Kneipp, H., Corio, P., Brown, S. D. M., Shafer, K., Motz, J., Perelman, L. T., Hanlon, E. B., Marucci, A., Dresselhaus, G. and Dresselhaus, M. S. (2000) *Phys. Rev. Lett.*, **84**, 3470.

36 Otto, A., Billmann, J., Eickmans, J., Ertuerk, U. and Pettenkofer, C. (1984) *Surf. Sci.*, **138**, 319.

37 Moskovits, M. (1985) *Rev. Modern Phys.*, **57**, 783.

38 Campion, A. and Kambhampati, P. (1998) *Chem. Soc. Rev.*, **27**, 241.

39 Kneipp, K., Kneipp, H., Kartha, V. B., Manoharan, R., Deinum, G., Itzkan, I., Dasari, R. R. and Feld, M. S. (1998) *Phys. Rev.*, **E57**, 6281.

40 Becke, A. D. (1993) *J. Chem. Phys.*, **98**, 5648.

41 Lee, C., Yang, W. and Parr, R. G. (1988) *Phys. Rev.*, **B37**, 785.

42 Frisch, M. J., Trucks, G. W., Schlegel, H. B., Scuseria, G. E., Robb, M. A., Cheesemann, J. R., Zakrzewski, V. G., Montgomery, J. A.Jr., Stratmann, R. E., Burant, J. C., Dapprich, S., Millam, J. M., Daniels, A. D., Kudin, K. N., Strain, M. C., Farkas, O., Tomasi, J., Barone, V., Cossi, M., Cammi, R., Mennucci, B., Pomelli, C., Adamo, C., Clifford, S., Ochterski, J., Petersson, G. A., Ayala, P. Y., Cui, Q., Morokuma, K., Malick, D. K., Rabuck, A. D., Raghavachari, K.,Foresman, J. B., Cioslowski, J., Ortiz, J. V., Baboul, A. G., Stafanov, B. B., Liu, G., Liashenko, A., Piskorz, P., Komaromi, I., Gomperts, R., Martin, R. L., Fox, D. J., Keith, T., Al-Laham, M. A., Peng, C. Y., Nanayakkara, A.,

Challacombe, M., Gill, P. M. W., Johnson, B., Chen, W., Wong, M. W., Andres, J. L., Gonzalez, C., Head-Gordon, M., Replogle, E. S. and Pople, J. A. computer code GAUSSIAN98 Revision A.9 (Gaussian Inc., Pittsburgh, PA, 1998)

43 Stewart, R. F. and Jensen, L. H. (1964) *J. Chem. Phys.*, **40**, 2071.

44 Denk, W., Strickler, J. H. and Webb, W. W. (1990) *Science*, **248**, 73.

45 Kawata, S., Sun, H.-B., Tanaka, T. and Takada, T. (2001) *Nature*, **412**, 667.

46 Shen, Y. R. (1984) *The Principles of Nonlinear Optics*, Wiley: New York.

47 Zumbusch, A., Holtom, G. R. and Xie, X. S. (1999) *Phys. Rev. Lett.*, **82**, 4142.

48 Hashimoto, M., Araki, T. and Kawata, S. (2000) *Opt. Lett.*, **25**, 1768.

49 Hashimoto, M. and Araki, T. (2001) *J. Opt. Soc. Am.*, A18, 771.

50 Cheng, J.-X., Volkmer, A. and Xie, X. S. (2002) *J. Opt. Soc. Am.*, **B19**, 1363.

51 Liang, E. J., Weippert, A.,Funk, J. M., Materny, A. and Kiefer, W. (1994) *Chem. Phys. Lett.*, **227**, 115.

52 Ichimura, T., Hayazawa, N., Hashimoto, M., Inouye, Y. and Kawata, S. (2003) *J. Raman Spectrosc.*, **34**, 651.

53 Ichimura, T., Hayazawa, N., Hashimoto, M., Inouye, Y. and Kawata, S. (2004) *Appl. Phys. Lett.*, **84**, 1768.

54 Hecht, B., Bielefeldt, H., Inouye, Y., Pohl, D. W. and Novotny, L. (1997) *J. Appl. Phys.*, **81**, 2492.

55 Boyd, G. T., Yu, Z. H. and Shen, Y. R. (1986) *Phys. Rev.*, **B33**, 7923.

56 Wilcoxon, J. P. and Martin, J. E. (1998) *J. Chem. Phys.*, **108**, 9137.

57 Tanaka, S., Cai, L. T., Tabata, H. and Kawai, T. (2001) *Jpn. J. Appl. Phys.*, **40**, L407.

58 For the estimation of the excited volume, the tip-enhanced local excitation spot was assumed to be a sphere with 20 nm diameter centered at the tip end in which the excitation efficiency is uniform. The locally excited volume is defined as the volume overlapped by the excitation spot and the sample. In these assumptions, the excited volume is approximately a column with 2.5 nm height and 20 nm diameter.

59 For the estimation of enhancement factor, CARS intensity of a DNA cluster without the silver tip was preliminarily measured, then the efficiency of the CARS emission per unit volume, peak power and repetition rate was estimated. Using the estimated efficiency, the enhancement factor is derived.